Supplement of Weather Clim. Dynam., 7, 1759–1778, 2026
https://doi.org/10.5194/wcd-7-1759-2026-supplement

Supplement of

Droughts in western Central Europe and associated atmospheric circulation patterns since 1844

Emile Neimry et al.

Correspondence to: Emile Neimry (emile.neimry@uclouvain.be)

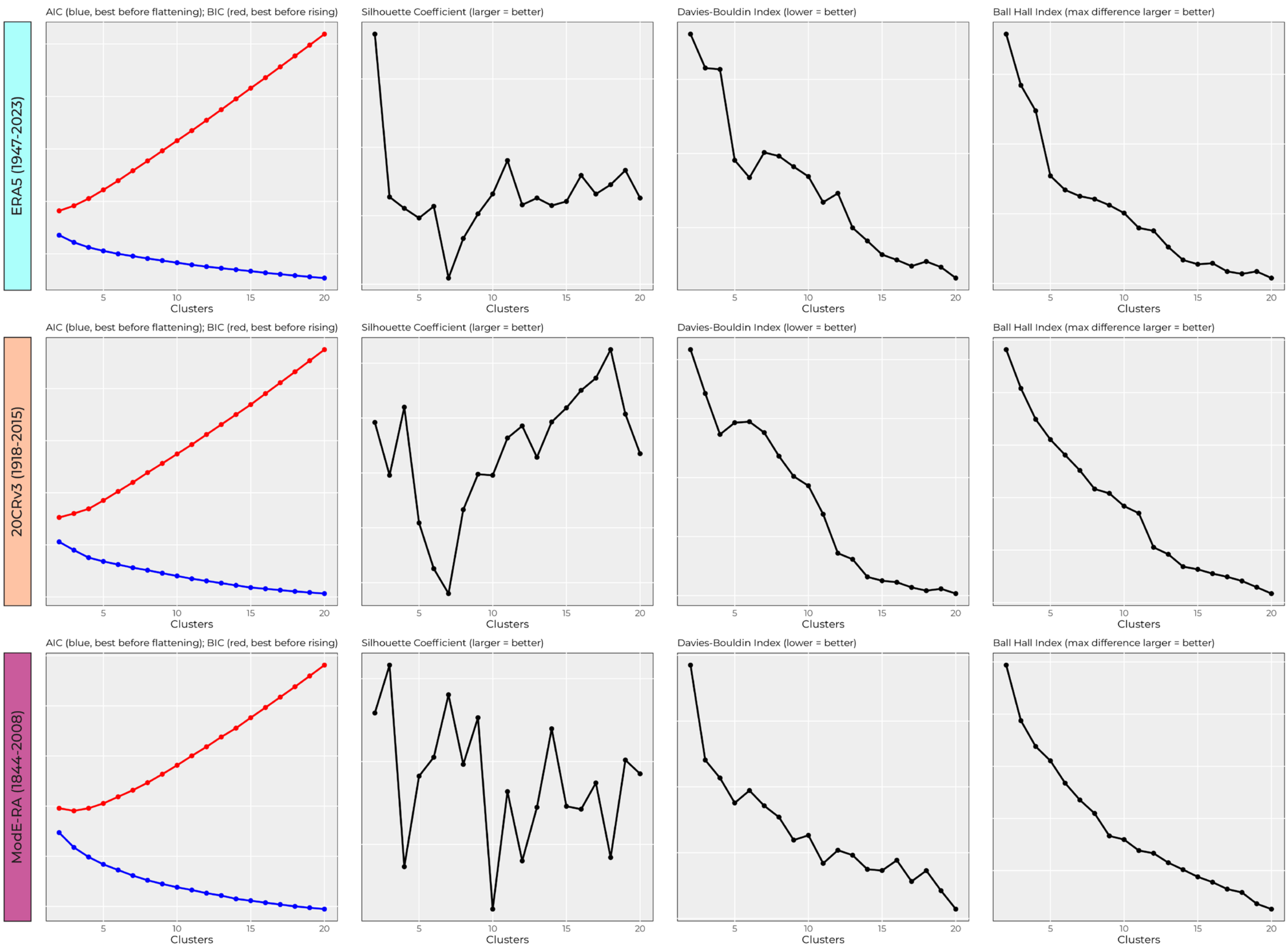

Figure S1. Clustering indices for two to twenty clusters (k) for each period–reanalysis combination (i.e. each row). The optimal criterion for each index is indicated in brackets. AIC: Akaike Information Criterion; BIC: Bayesian Information Criterion.

Table S1. Summary of weather stations selected for data evaluation. The maximum continuous years within the specified period are indicated in bold.

Weather Stations	Period covered for temperature (T)	Period covered for precipitation (P)	Commun period for both T and P	Latitude	Longitude	Altitude	Sources
Uccle (BE)	1833 - 2023 **(191)**	1833 - 2023 **(191)**	1833 - 2023 **(191)**	50.80° N	4.40° E	100 m	RMI
De Bilt (NL)	1706 - 2018 **(313)**	1849 - 2018 **(170)**	1849 - 2018 **(170)**	52.10° N	5.18° E	2 m	KNMI Climate Explorer
Frankfurt am Main (DE)	1757 - 1961 **(205)**	1826 - 2000 **(175)**	1826 - 1960 **(135)**	50.10° N	8.70° E	109 m	
Paris-Le Bourget (FR)	1757 - 2000 **(244)**	1770 - 2004 **(235)**	1770 - 2000 **(231)**	48.80° N	2.50° E	50 m	

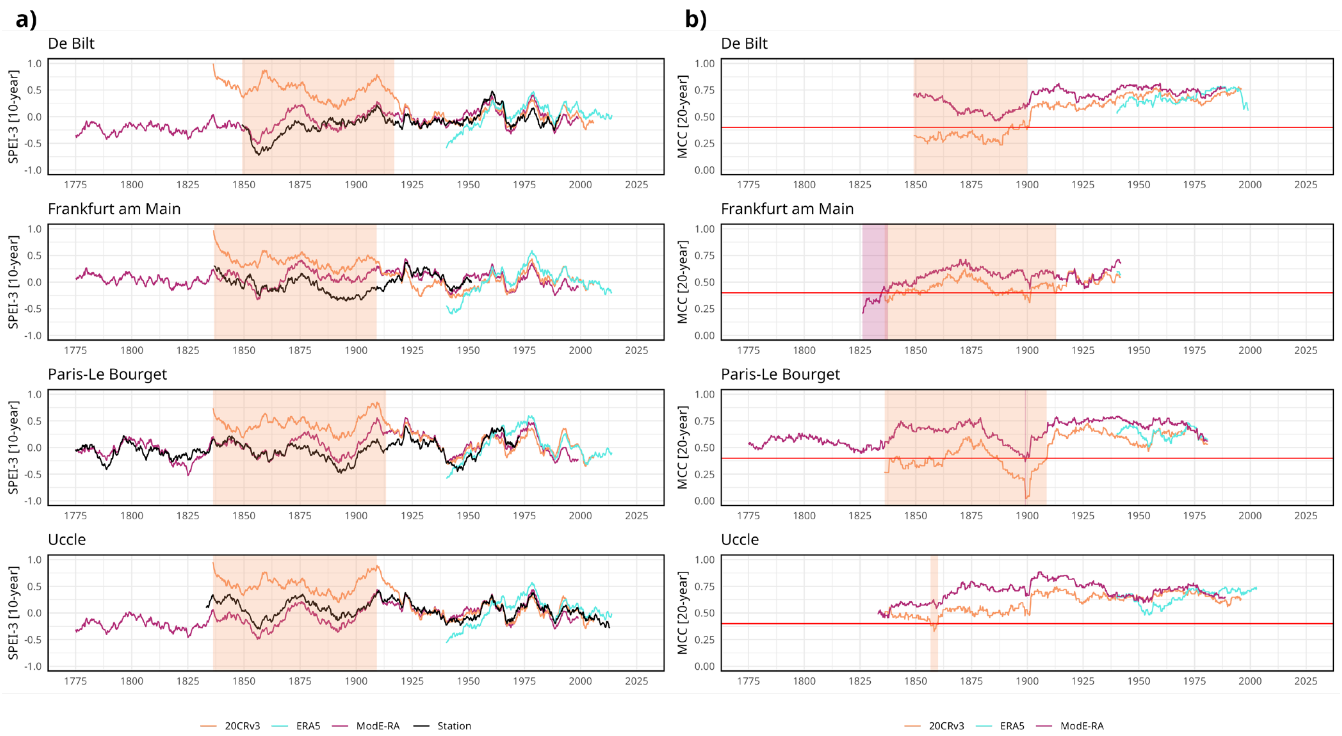

Figure S2. Same as Fig. 1, but for SPEI-3.

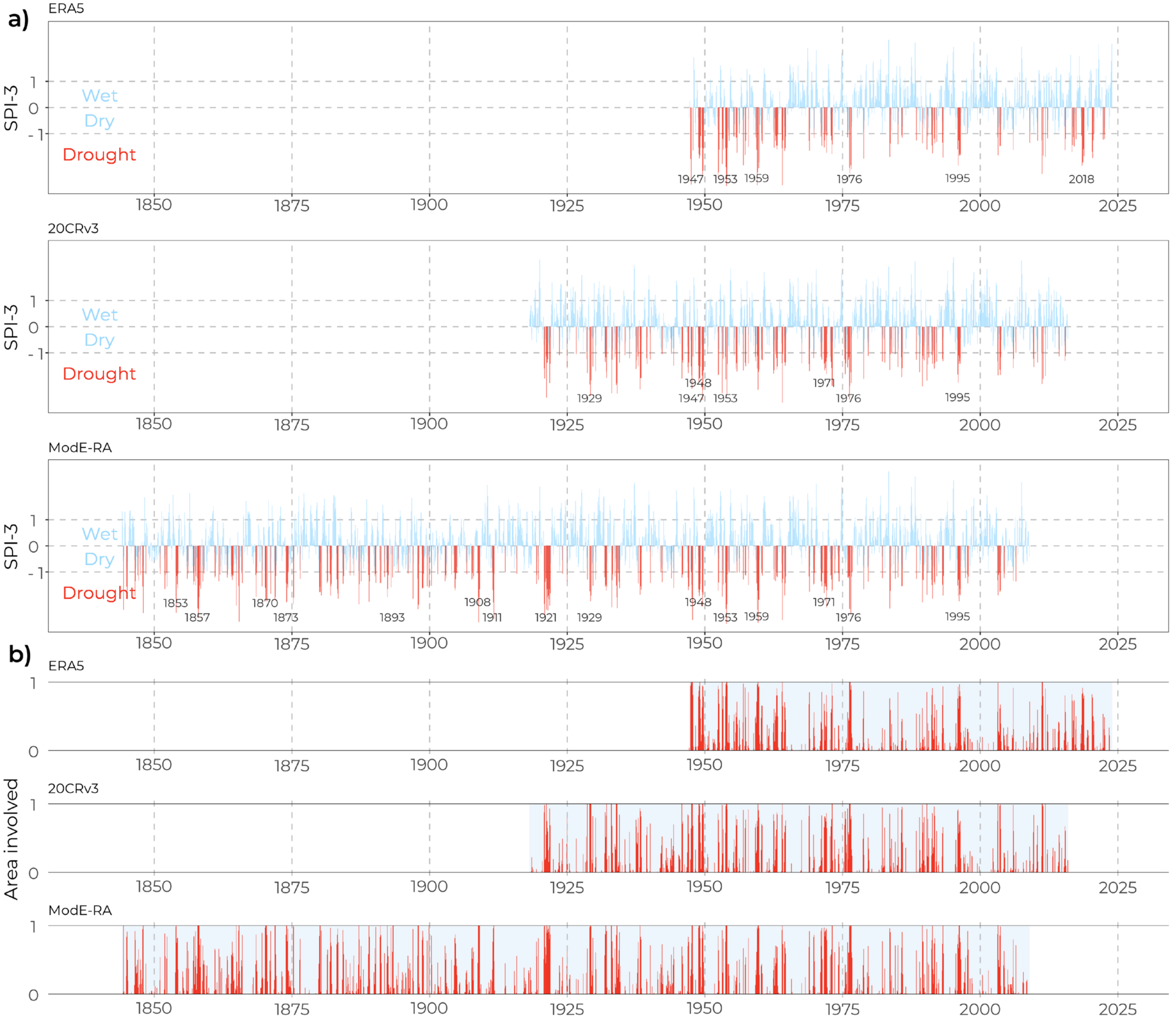

Figure S3. Same as Fig. 2, but for SPI-3.

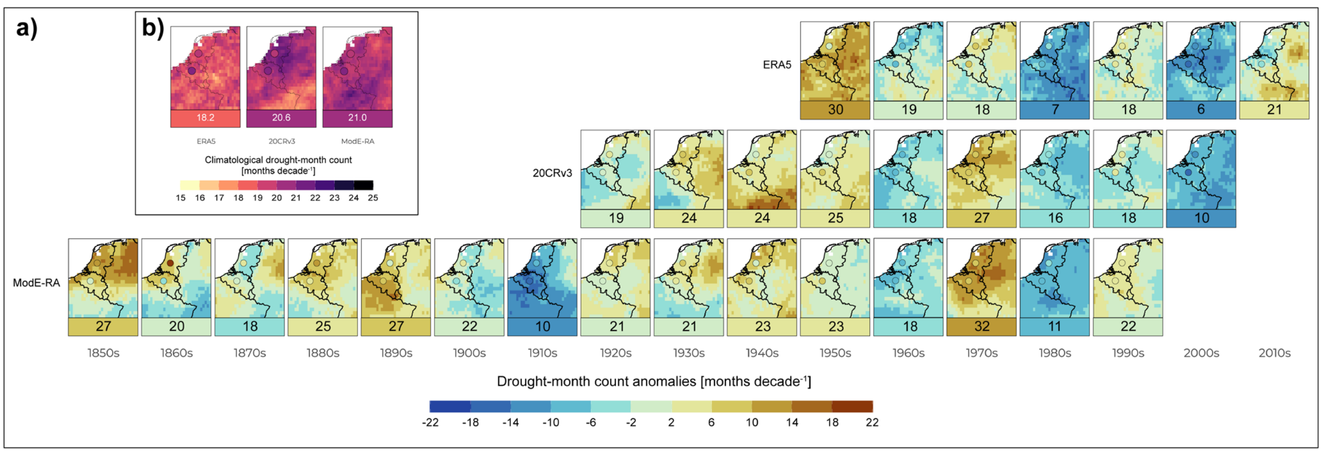

Fig. S4. Same as Fig. 3, but for SPI-3

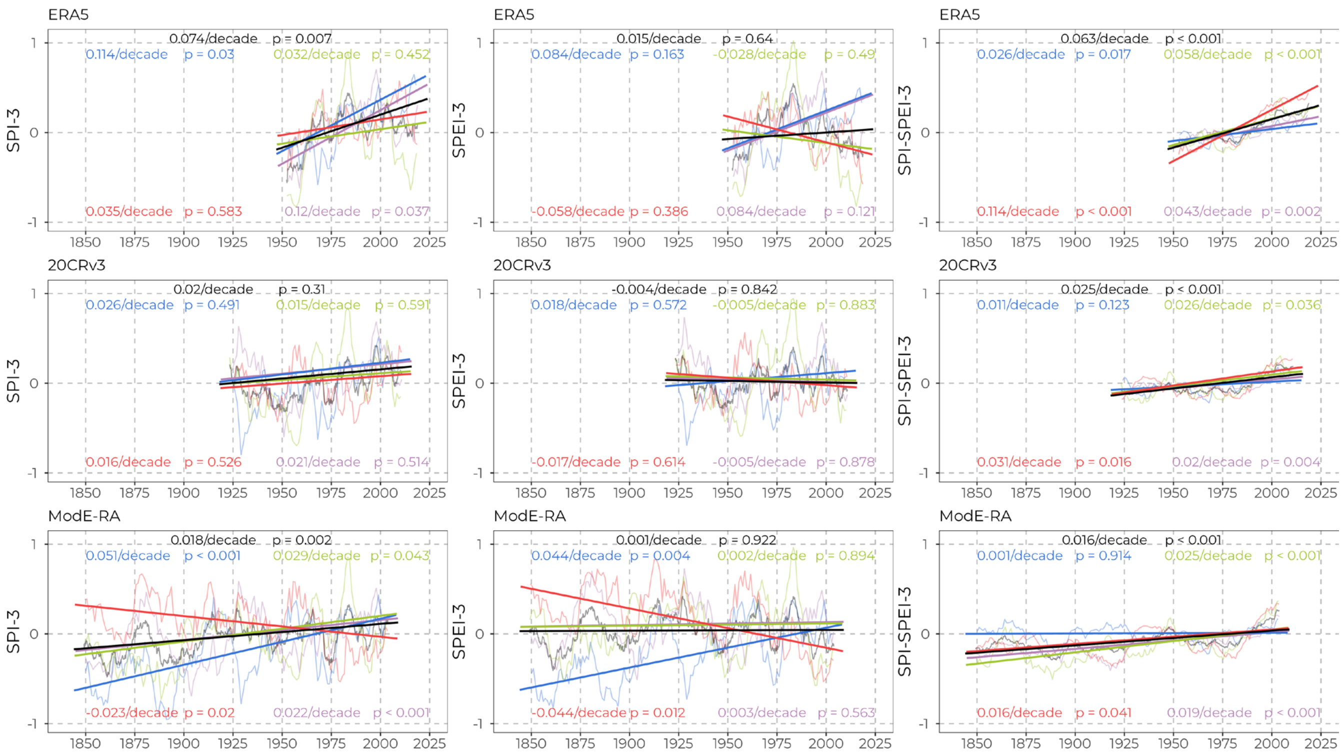

Figure S5. 10-year moving average time series of year-round and seasonal SPI-3 (first column), SPEI-3 (second column), and their difference (SPI-3 minus SPEI-3; third column) in western Central Europe for each dataset (rows). Black, blue, green, red, and purple represent year-round, winter, spring, summer, and autumn trends, respectively. The difference between SPI-3 and SPEI-3 provides an indicator of the relative contribution of atmospheric evaporative demand (AED) to climatic water balance anomalies. Straight lines show Sen's slopes calculated from the raw monthly index values rather than the 10-year moving averages. The corresponding p-values from the MMKH trend tests, also calculated from the raw monthly values, are shown for the year-round and seasonal series in their respective colours.

Table S2. Trends in 3-month drought parameters based on the Sen's slope relative to the climatology (1947-2008) per °C of warming. Values in bold are the ones with a MMKH p-value below 0.05.

	3-month precipitation trend *(% C⁻¹)*			**3-month AED trend *(% C⁻¹)***			**3-month mean temperature trend (°C decade⁻¹)**		
	1844-2008 (ModE-RA)	1918-2015 (20CRv3)	1947-2023 (ERA5)	1844-2008 (ModE-RA)	1918-2015 (20CRv3)	1947-2023 (ERA5)	1844-2008 (ModE-RA)	1918-2015 (20CRv3)	1947-2023 (ERA5)
All months	***6.0***	*5.7*	***8.3***	***8.4***	***9.2***	***9.4***	**0.06**	**0.09**	**0.23**
Winter	***17.5***	*12.5*	***12.1***	***25.8***	*23.5*	***33.0***	**0.06**	0.06	**0.25**
Spring	***9.2***	*3.3*	*3.5*	***10.9***	***10.6***	***11.5***	**0.05**	**0.09**	**0.21**
Summer	***-7.2***	*3.8*	*2.9*	***5.9***	***6.3***	***6.4***	**0.06**	**0.09**	**0.28**
Autumn	***7.5***	*6.4*	***20.2***	***9.5***	**8.7**	***9.9***	**0.06**	**0.09**	**0.15**

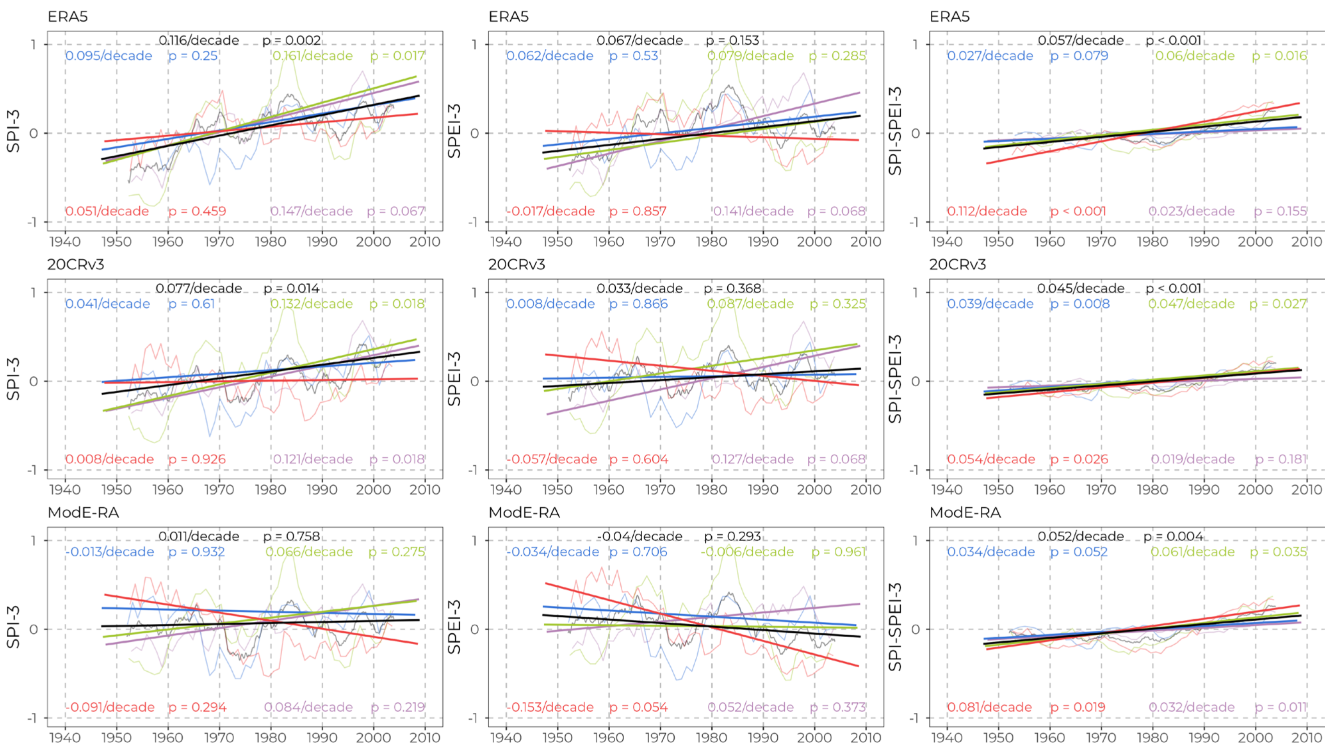

Figure S6. Same as Fig. S5, but over the common period (1947-2008).

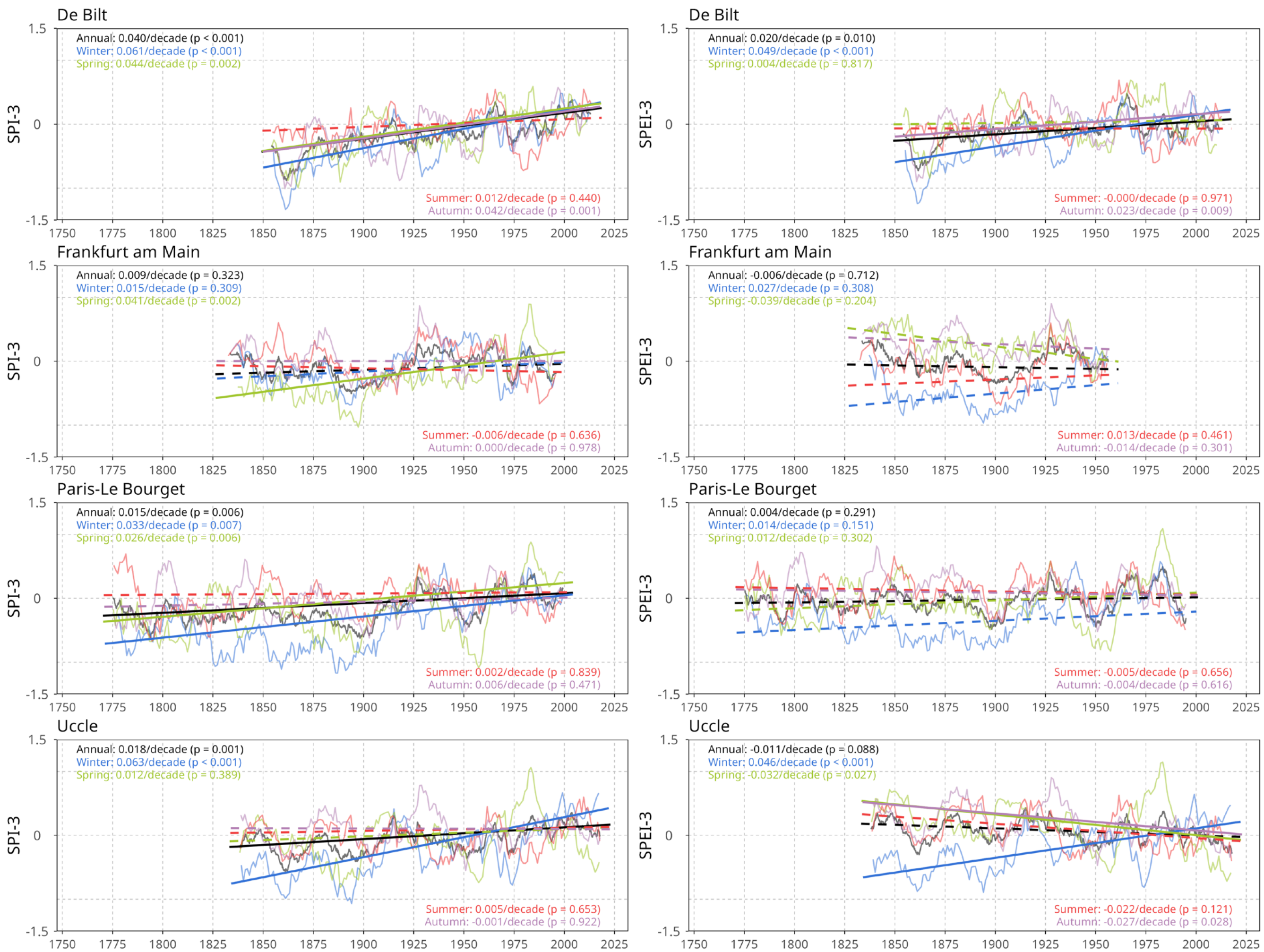

Figure S7. Seasonal trends in SPI-3 (left) and SPEI-3 (right) at the four stations. Coloured lines represent 10-year moving averages for the individual seasons and the annual series, while solid and dashed lines indicate significant (*p* < 0.05) and non-significant Sen's slope trends based on the modified Mann–Kendall test, respectively. Trend magnitudes (per decade) and associated *p*-values are shown within each panel.

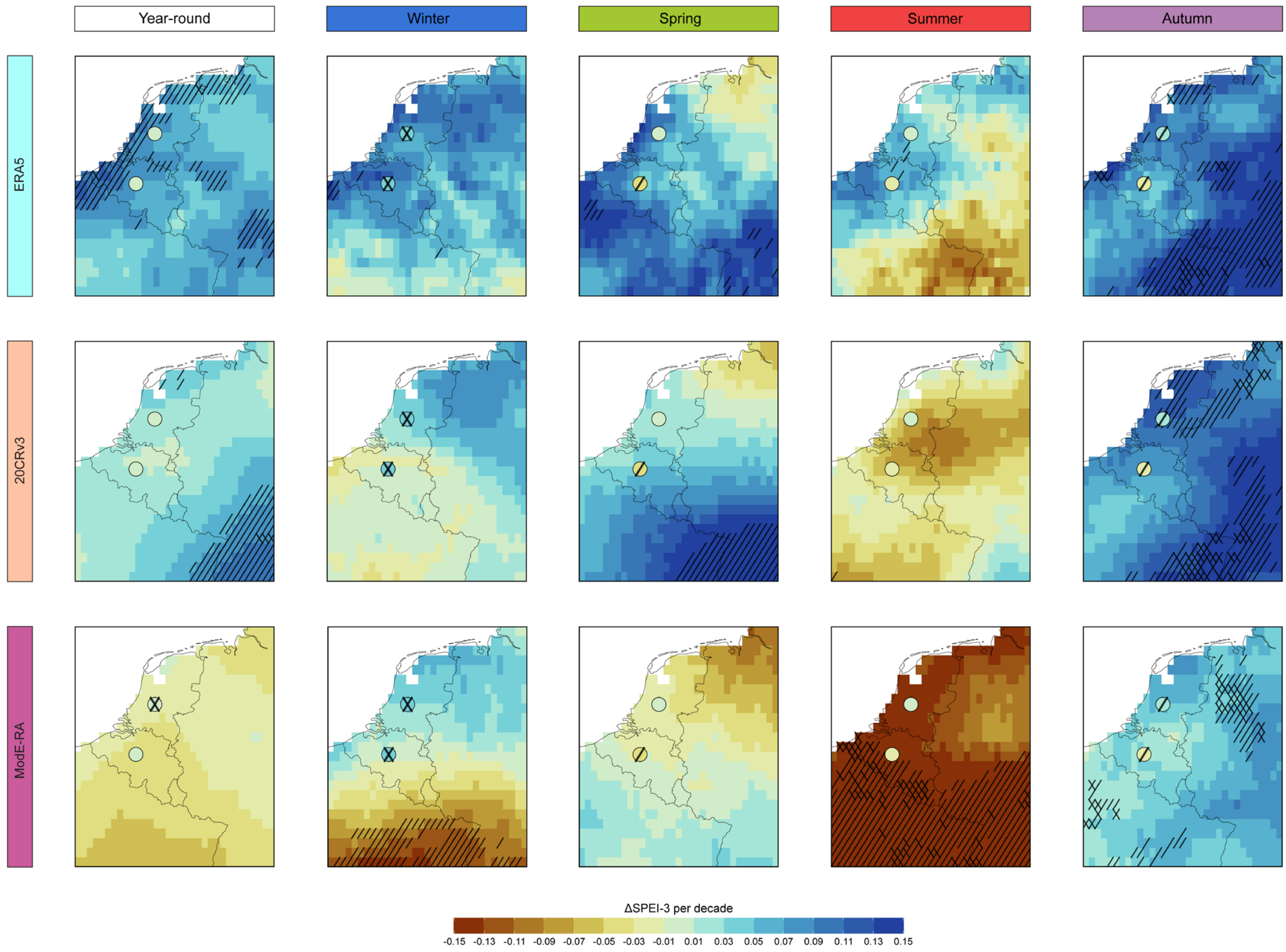

Figure S8. Year-round (first column) and seasonal (winter, spring, summer, and autumn; second to fifth columns) dryness trends during the reference period (1947–2008) for SPEI-3, shown for each period–reanalysis combination (one row per combination). Circles indicate the corresponding values from weather station observations. A single diagonal line indicates a modified Mann–Kendall test *p*-value < 0.05, whereas two crossing diagonal lines indicate *p* < 0.001.

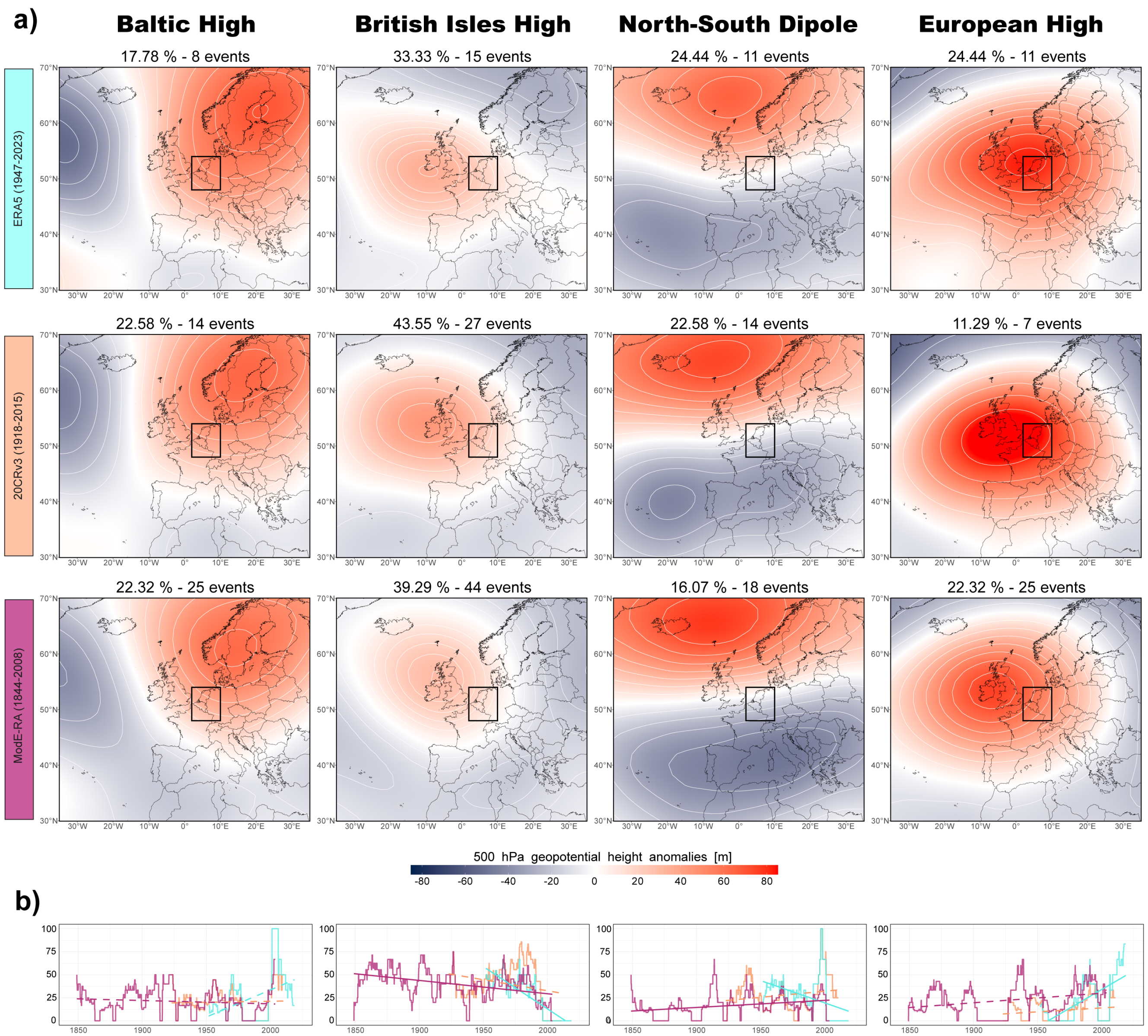

Figure S9. Same as Fig. 5 but related to SPI-3 drought-based clustering.

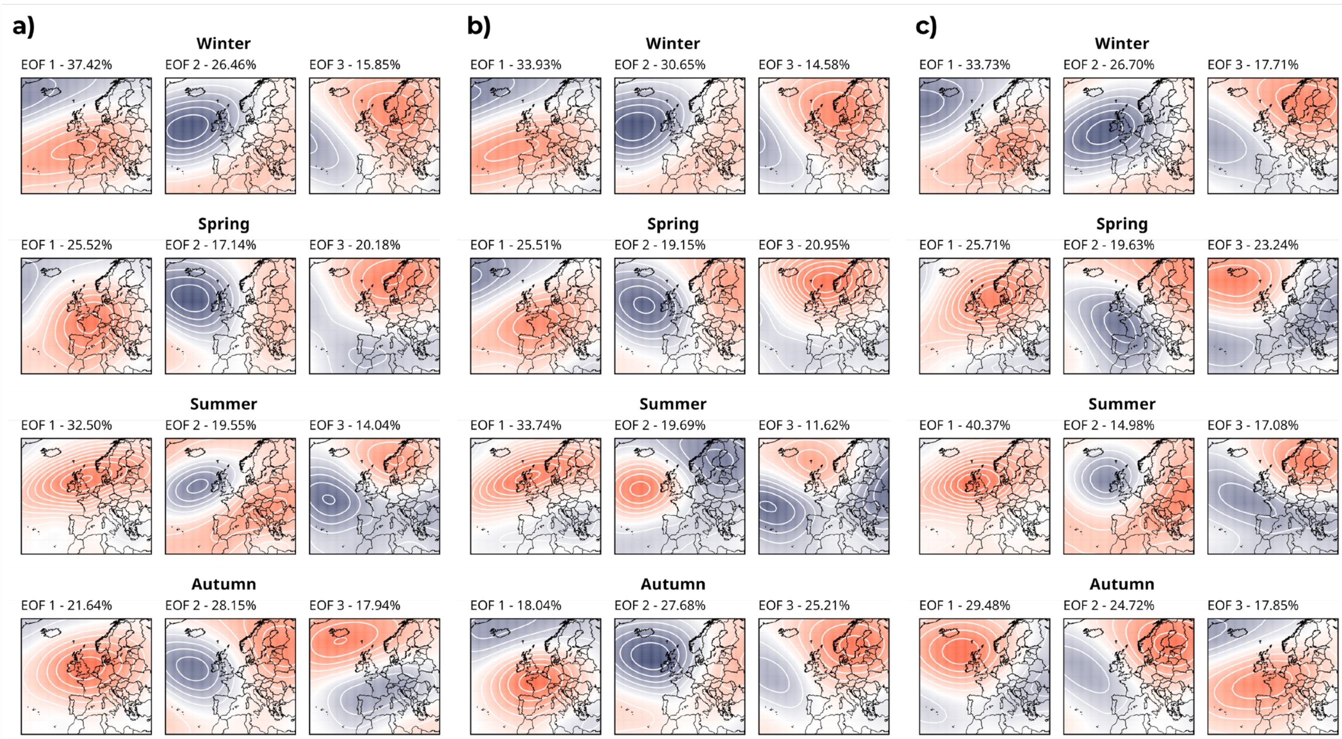

Figure S10. Seasonal EOF patterns of 500 hPa geopotential height anomalies computed from the full available record for (a) ERA5 (1947–2023), (b) 20CRv3 (1918–2015), and (c) ModE-RA (1844–2008).

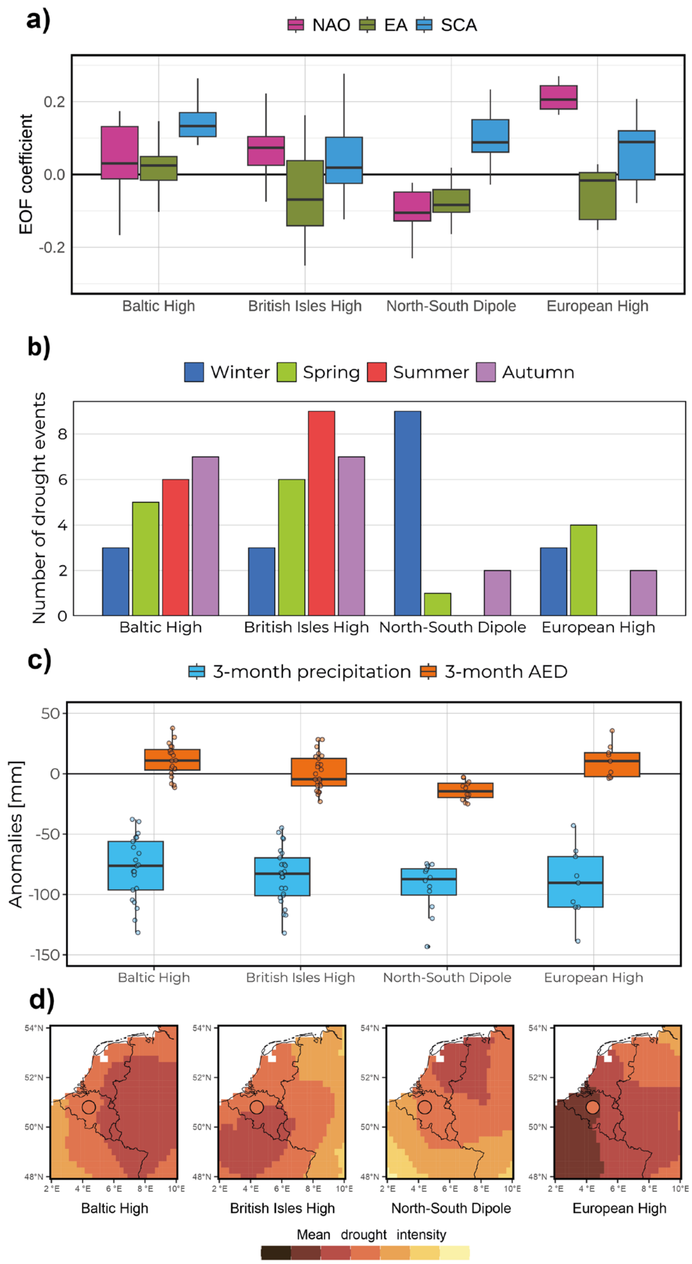

Figure S11. Same as Fig. 6, but over 1918-2015 (20CRv3).

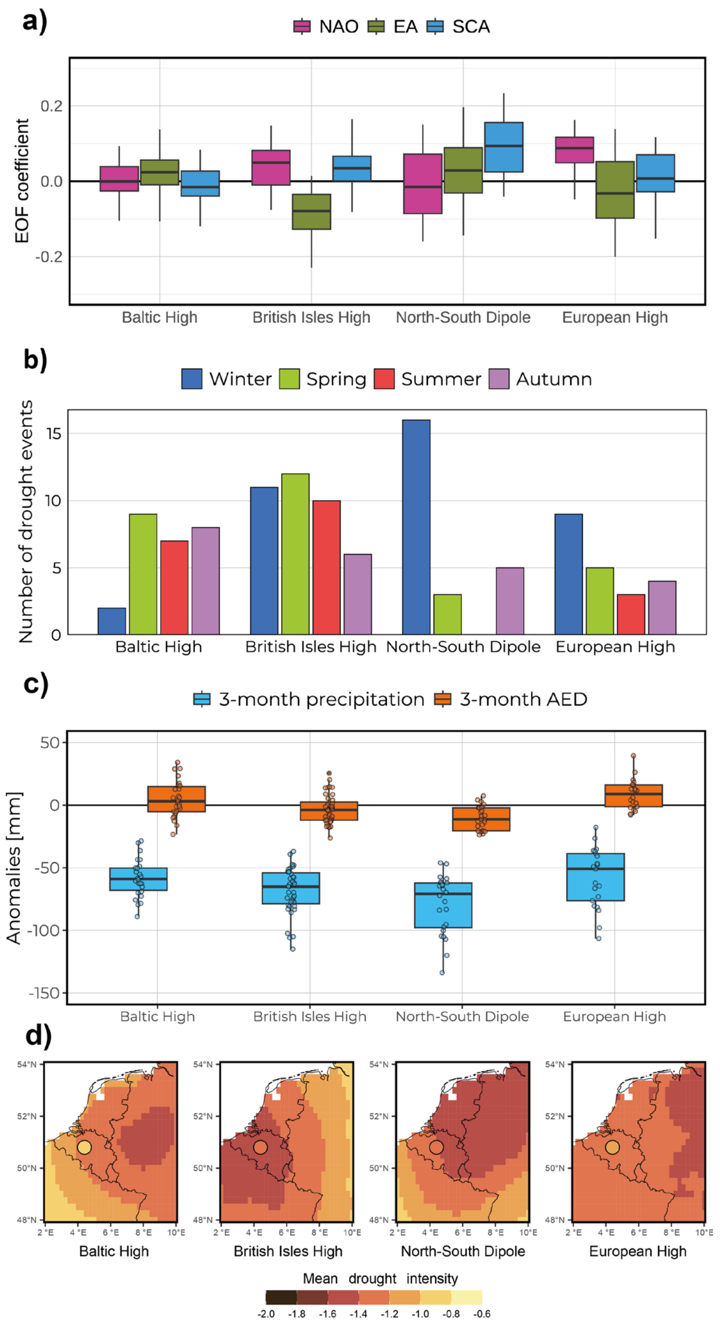

Figure S12. Same as Fig. 6, but over 1844-2008 (ModE-RA).

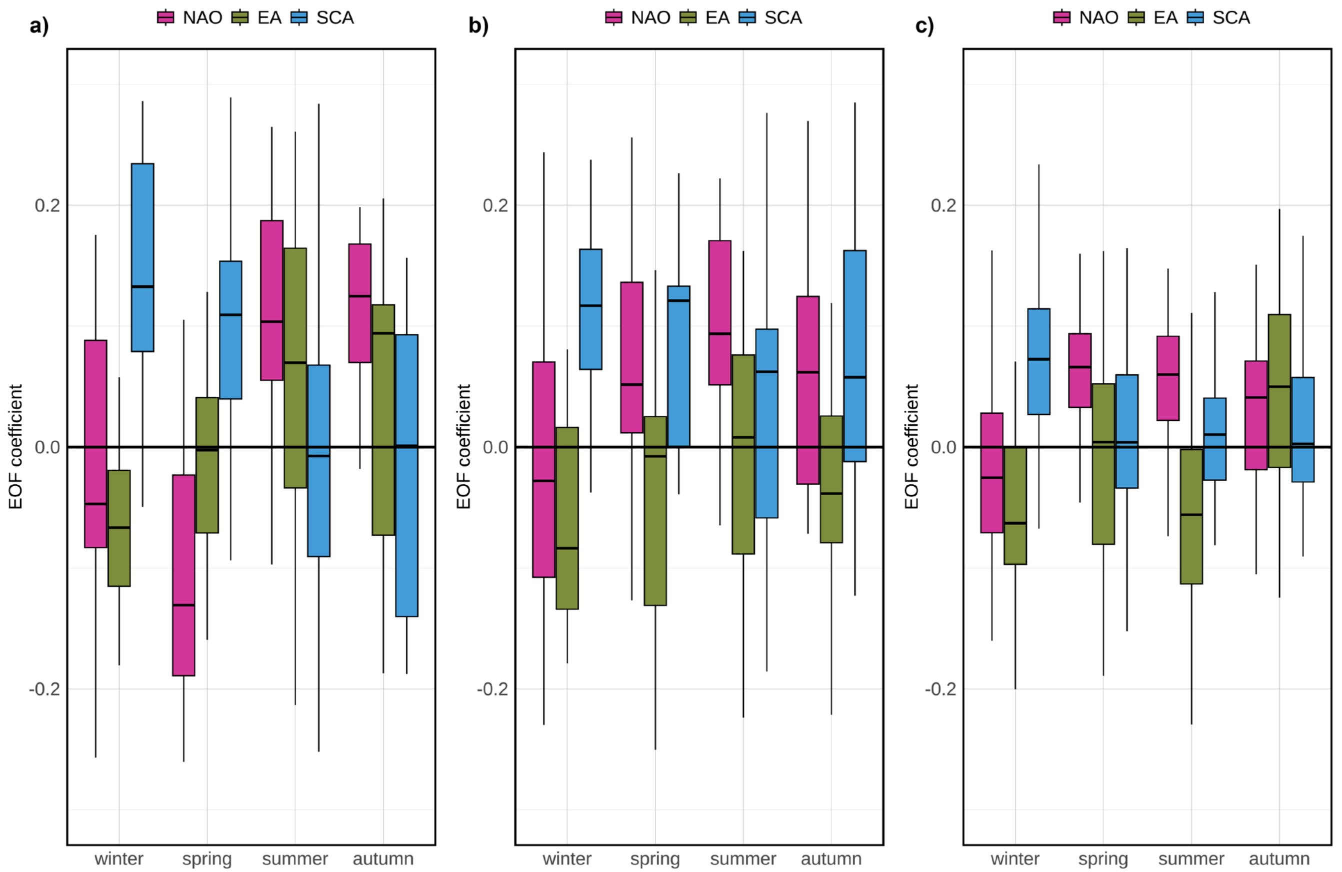

Figure S13. Seasonal EOF coefficients for SPEI-3 droughts over (a) 1947–2023 for ERA5, (b) 1918–2015 for 20CRv3, and (c) 1844–2008 for ModE-RA.

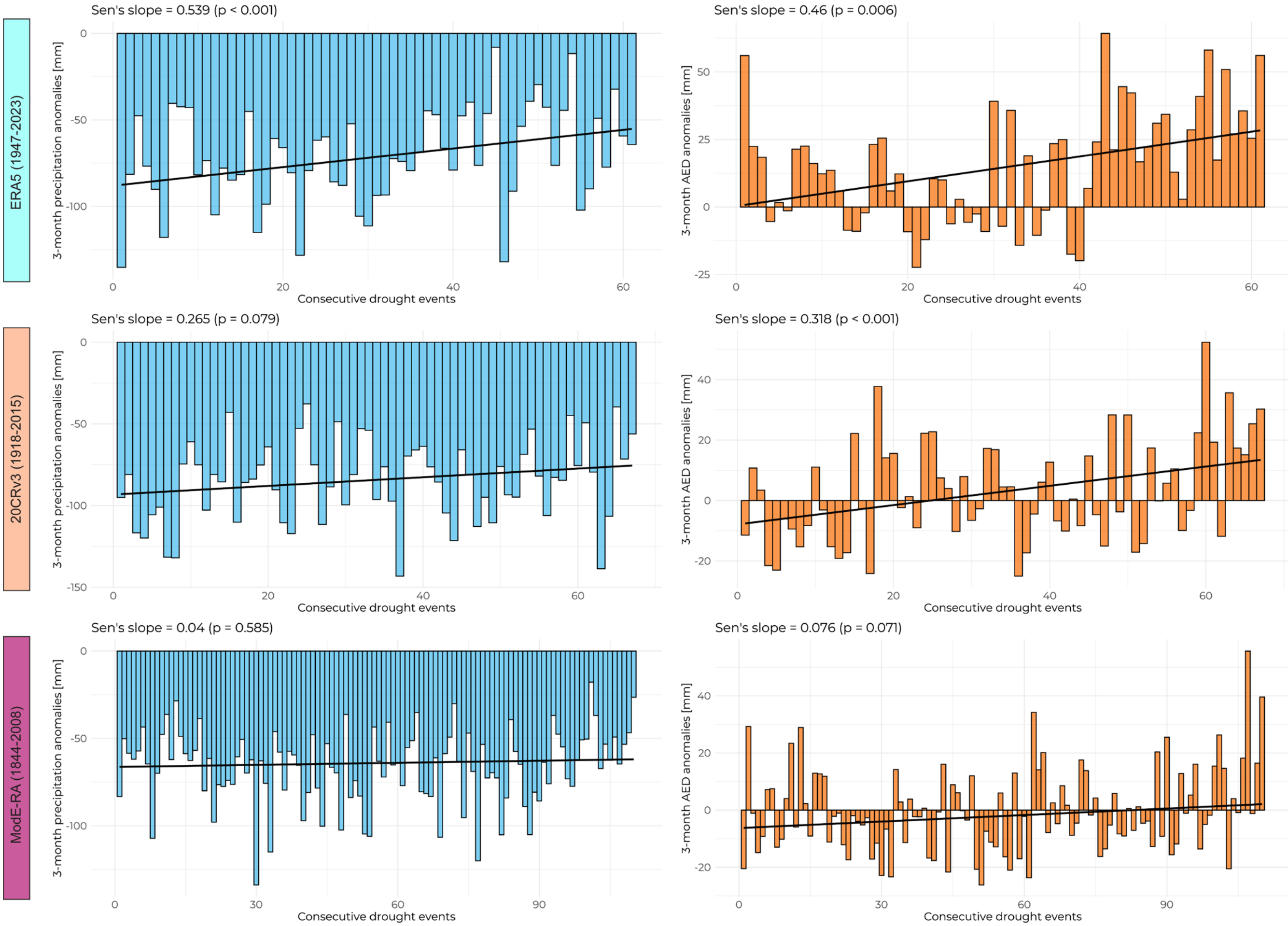

Figure S14. Evolution of 3-month precipitation (left) and potential evapotranspiration (right) anomalies associated with drought events for each period–reanalysis combination (one row per combination). The x-axis represents a concatenated sequence of identified drought events and therefore does not correspond to a continuous time series.

S1. Supplementary Evaluation: atmospheric evaporative demand formulation

Atmospheric evaporative demand (AED) is estimated in the present study using the Thornthwaite method (Thornthwaite, 1948). This formulation depends only on air temperature and latitude, allowing AED to be calculated consistently across all three reanalysis datasets despite differences in the variables they provide. The Penman–Monteith method (Penman, 1948), particularly the FAO-56 formulation (Allen et al., 1998), is generally considered the standard approach for estimating reference evapotranspiration because it more explicitly represents the physical controls on evaporation. It incorporates net radiation, soil heat flux, air temperature, wind speed, vapour pressure, the slope of the saturation vapour pressure curve, and the psychrometric constant.

The sensitivity of the results to the AED formulation is evaluated using ERA5, where the strongest recent warming is expected to maximise differences between Thornthwaite- and Penman–Monteith-derived AED estimates. Drought identification is only weakly affected by the choice of formulation, with excellent agreement between Thornthwaite- and Penman–Monteith-based SPEI (MCC = 0.86) over 1947–2023. Similarly, agreement between SPEI derived from ERA5 at the Uccle grid point and the Uccle station record remains comparable for both formulations (MCC = 0.65 for Thornthwaite and 0.61 for Penman–Monteith). The slightly higher agreement obtained using Thornthwaite may reflect the additional uncertainties introduced by the larger number of meteorological variables required by the Penman–Monteith formulation, particularly radiation and wind speed, which are generally less reliably observed than temperature (Trenberth et al., 2014).

Long-term hydroclimatic trends are only marginally influenced by the choice of AED formulation (Fig. S15). Thornthwaite generally produces slightly larger increases in AED than Penman–Monteith (Fig. S15a), affecting the magnitude but not the direction of SPEI trends (Fig. S15b). Consequently, the conclusions regarding seasonal and annual drought evolution remain unchanged. Relative differences between the two formulations are largest during winter and autumn, when evapotranspiration estimates are most sensitive to the choice of PET formulation under energy-limited conditions (Hobbins et al., 2008). However, because AED contributes less to drought variability during these seasons than during spring and summer, the overall interpretation remains unchanged.

Atmospheric circulation patterns associated with drought events are also nearly identical when Penman–Monteith-derived SPEI is used, indicating that the identification of the dominant circulation regimes is robust to the choice of AED formulation.

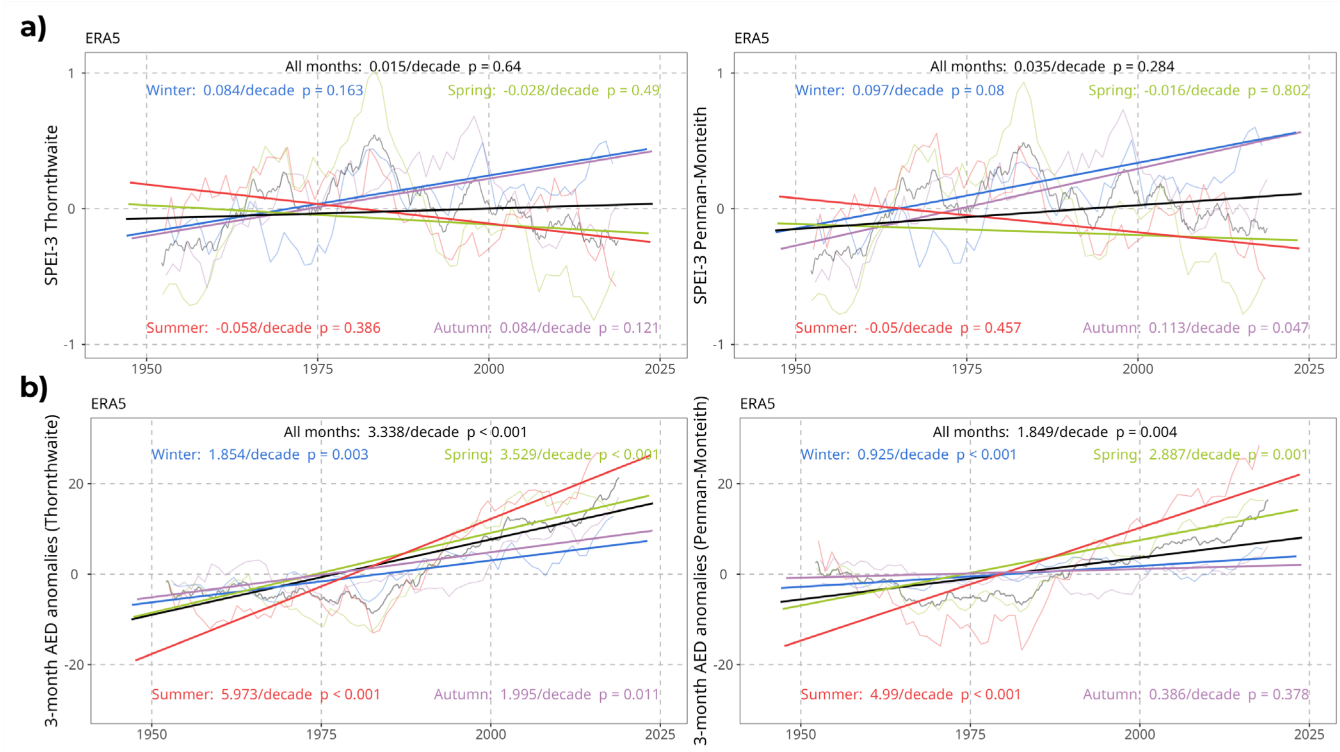

Figure S15. 10-year moving average time series of year-round and seasonal (a) SPEI-3 values calculated using the Thornthwaite and Penman–Monteith formulations and (b) 3-month AED anomalies calculated using the Thornthwaite (left) and Penman–Monteith (right) formulations over western Central Europe from ERA5. Straight lines represent Sen's slopes calculated from the raw monthly values rather than from the 10-year moving averages.

References of the Supplement

Allen, R. G., Pereira, L. S., Raes, D., & Smith, M. (1998). Crop evapotranspiration-Guidelines for computing crop water requirements-FAO Irrigation and drainage paper 56. *Fao, rome*, *300*(9), D05109.

Hobbins, M. T., Dai, A., Roderick, M. L., & Farquhar, G. D. (2008). Revisiting the parameterization of potential evaporation as a driver of long-term water balance trends. *Geophysical Research Letters*, *35*(12).

Penman, H. L. (1948). Natural evaporation from open water, bare soil and grass. *Proceedings of the royal society of London. Series A. Mathematical and physical sciences*, *193*(1032), 120-145.

Thornthwaite, C. W. (1948). An approach toward a rational classification of climate. *Geographical review*, *38*(1), 55-94.

Trenberth, K. E., Dai, A., Van Der Schrier, G., Jones, P. D., Barichivich, J., Briffa, K. R., & Sheffield, J. (2014). Global warming and changes in drought. *Nature Climate Change*, *4*(1), 17-22.